The evolution of turbulence characteristics in the wake of a horizontal axis tidal stream turbine

Mohammad H. B. Ahmadi*, Zhiyin Yang

School of Mechanical Engineering and the Built Environment, University of Derby, Derby, DE22 3AW, UK

Abstract

The evolution of turbulence characteristics downstream of a laboratory-scale three-bladed horizontal axis turbine is investigated in this study. Large eddy simulation (LES) coupled with the Actuator Line Modelling (ALM) is used to simulate the flow. The numerical results compare well against experimental data, which shows that the LES/ALM technique is a powerful tool for simulating tidal stream turbines. The present study aims to obtain a better understanding of the turbulence characteristics of flow in the turbine wake by removing deterministic velocity fluctuations stemmed from the turbine rotation. Large eddy simulation is able to provide high-resolution spatial and temporal information needed for this work. The filtering process helps to have a clearer view of the flow structures downstream by tracking the streamwise variations of turbulence intensity and turbulent kinetic energy and, reveals a transition zone started shortly behind the turbine with a peak in the turbulence intensity. This study introduces turbulence intensity and turbulent kinetic energy as quantitative criteria to split the turbine wake into distinct regions. This research shows that to investigate and explain the influence of different upstream and operation conditions on the flow characteristics in the turbine wake, a well understanding of flow characteristic changes in the transition zone is necessary.

Keywords: Tidal stream turbine, Actuator line method, Large eddy simulation, Turbulence intensity, Turbulent kinetic energy, Deterministic velocity fluctuations

1. Introduction

The interest in tidal stream energy worldwide is increasing due to a number of attractive features. It is a renewable and clean form of energy with a regular and predictable periodicity which makes it a more reliable source of energy in comparison to waves and wind. At the moment, the marine energy industry has lagged far behind as energy source. There are still many scientific and technological challenges to be overcome before the identified potential of marine energy can be fulfilled. Within the next decade it is likely that large-scale energy extraction of tidal energy at specific sites will be undertaken and tidal arrays will be deployed in order to generate considerable power. However, there are still many features to be studied in more details for designing turbine arrays. For example, the flow approaching downstream turbines is often highly

*Corresponding author

Email addresses: m.ahmadi@derby.ac.uk (Mohammad H. B. Ahmadi), z.yang@derby.ac.uk (Zhiyin Yang)

turbulent and consequently their blade loading, power output and wake characteristics experience continuous variations. These effects could play an important role in designing and optimising turbine proximity and array configuration. The motivation for studying the wake of Tidal Stream Turbines (TSTs) is to understand how it influences device proximity and net power output from turbines in an array and individual device loading.

There have been many studies of flow characteristics in the near and far wake of an axial flow turbine. Afgan *et al.* [1] studied coherent tip vortices which break up downstream using large eddy simulation. Kang *et al.* [2] showed that the meandering of the instantaneous turbine wake is reinforced considerably by the interactions of the inner wake and the outer wake due to the blade tip vortices resulting in destroying the swirling flow in the wake rapidly and increasing the size and streamwise extent of the wake meandering region. Tedds *et al.* [3] revealed the strongly anisotropic nature of the near wake turbulence. Chamorro *et al.* [4] showed the turbulence intensity distribution is highly heterogeneous downstream and its evolution around the turbine tip provides evidence about the spreading of the wake and the loss of stability of the vortical structures. Nuernberg *et al.* [5]showed that in areas of lower ambient turbulence levels, wake velocity and turbulence recovery are strongly linked and wake recovery is more significantly affected by the lateral proximity particularly towards the front rows of the array. Bahaj *et al.* [6] showed that the close proximity of both water surface and seabed has a strong influence on the flow structure downstream of a TST. Chen *et al.* [7] studied the wake structure of a single turbine and showed that the wake turbulence is strong and anisotropic and, the velocity deficit behind the turbine is mainly induced by the kinetic energy extraction and the blockage effects of the rotor and support structure. Stallard *et al.* [8] studied the performance and flow characteristics of a group of three-bladed rotors in a wide flume to improve our current understanding of wake interaction in turbine arrays. There are also many studies about wind turbine wakes including experimental works by Medici *et al.* [9], Sherry *et al.* [10] and Ozbay *et al.* [11] and computational studies by Abkar *et al.* [12] and Xie *et al.* [13]. In their studies, various wake details have been analysed including tip vortex generation and break up, and large scale wake meandering.

In spite of these studies, however, many basic characteristics of flow remain today poorly understood. For example, whilst the mean flow velocities are reasonably well understood, our understanding of turbulence characteristics in the near wake, particularly the transition zone and the region leading to it is lacking. In experimental studies, due to practical restrictions, in most measurements the region behind the turbine leading to the transition zone is absent or partly covered [3, 4, 7]. To the author's best knowledge, the experimental data disseminated by Jordan *et al.* [14] is the only experiment on horizontal axis TST presenting data from the upstream up to 5D downstream of the turbine covering the transition zone which is considered as the benchmark in this study, to validate the numerical results.

Similarly, as reported by Batten *et al.* [15], numerical simulations using the actuator disc modelling (ADM) and the blade element momentum (BEM) theory [15] are not able to represent the near wake of the turbine accurately because of their nature and weakness in predicting hub/tip vortices. Nilsson *et al.* [16]

and Martinez *et al.* [17] have shown that ALM can be considered as a good choice to simulate the near wake by capturing hub/tip vortices which makes it capable of predicting the wake expansion, the circulation and the velocity distributions with satisfying results.

On the other hand, in the near wake especially near the turbine plane, due to the strong influence of turbine rotation, velocity fluctuations consist of both deterministic and turbulent components and to evaluate turbulence characteristics, deterministic velocity fluctuations (DVFs) have to be filtered out [18, 19]. Fortunately, large eddy simulation is potentially able to provide high-resolution spatial and temporal information needed for filtering DVFs.

In literature, turbine wakes are typically divided into a near wake and a far wake. However, there is no unique definition to separate them. Most definitions generally suppose that turbulence and vorticity generated at the rotor are diffused in the near wake, resulting in more evenly distributed turbulence and velocity profiles in the far wake [20]. For example, Myers & Bahaj [21] define the downstream limit of the near wake as the point at which the shear layer developed between the wake and the free stream reaches the wake centreline. This study shows that the turbine wake can be split into distinct regions according to the streamwise variations of the turbulence intensity.

Besides the evaluation of numerical results by comparing against experimental data, this paper aims to provide a better view of the evolution of turbulence characteristics in the turbine wake, particularly in the transition zone and the region leading to it when DVFs being filtered out. The hybrid LES/ALM technique used here has already been validated and correlated well with the experimental measurements [22, 23].

2. Numerical modelling

2.1. Large eddy simulation

In LES only large eddies (large scale motions) are computed directly and hence a low-pass spatial filter is applied to the instantaneous conservation equations (Navier-Stokes) to formulate the three dimensional unsteady governing equations for large scale motions. The effects of small scale motions are modelled using a subgrid-scale (SGS) model.

The filtered equations expressing conservation of mass and momentum for incompressible flow can be written in conservative form as:

$$\frac{\partial \bar{u}_i}{\partial x_i} = 0 \tag{1}$$
$$\frac{\partial \bar{u}_i}{\partial t} + \frac{\partial (\bar{u}_i \bar{u}_j)}{\partial x_j} = -\frac{1}{\rho}\frac{\partial \bar{p}}{\partial x_i} + \nu \frac{\partial^2 \bar{u}_i}{\partial x_j^2} + \frac{\partial \tau_{ij}}{\partial x_j} + f_{i,\epsilon}$$

where the bar denotes filtering and $f_{i,\epsilon}$ is the body force calculated from the ALM technique described briefly in Section. 2.2 The sub-grid scale turbulent stresses are modelled with an eddy viscosity as:

$$\tau_{ij} = -\nu_t \left(\frac{\partial \bar{u}_i}{\partial x_j} + \frac{\partial \bar{u}_j}{\partial x_i} \right) + \frac{2}{3} k \delta_{ij} \tag{2}$$

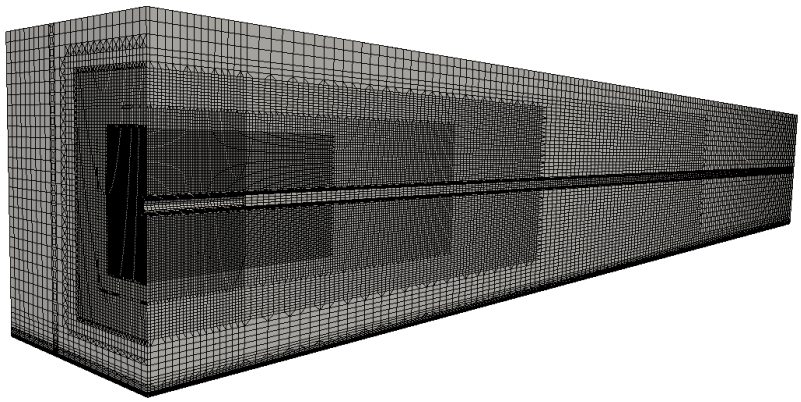

Figure 1: A perspective view of the computational mesh cut a the turbine and vertical centre planes.

where ν_t and k denote the eddy viscosity and sub-grid kinetic energy respectively and are determined using the one-equation eddy viscosity model in which an extra equation for the sub-grid turbulent kinetic energy [24] is solved. The filtered governing equations are solved using the CFD code library OpenFOAM [25].

2.2. Actuator line modelling

The geometry of the turbine blades is not directly resolved in the current study and is represented using the ALM technique originally developed by Sørensen & Shen [26]. In the ALM technique, along rotating actuator lines representing the turbine blades, body forces equal and opposite to the lift and drag forces experienced by the turbine are imposed on the flow. At each time step, initially, full 3D LES governing equations are solved to obtain the flow field. With the availability of the flow field, the blade geometry and a table of 2D airfoil characteristics, C_L and C_D as functions of Reynolds number and angle of attack, the loads on the rotor blades are calculated using a blade element approach. A correction factor introduced by Shen *et al.* [27] is applied on the computed 2D forces to take 3D rotational effects into account. The corrected body forces are then projected smoothly along the actuator lines and neighbouring mesh points using a Gaussian function to avoid singular behaviour and numerical instability. In the present study, the Gaussian cut-off parameter is constant and has a value between 2 and 3 cell sizes [28]. Details of the ALM technique used in the present study can be found in [23].

2.3. Computational domain

A horizontal axis laboratory scale TST comprising of three blades with a 0.2 m diameter has been numerically simulated with the hybrid LES/ALM technique. The geometrical and model specifications are determined based on the experimental set up of Jordan *et al.* [14]. The Experiment was performed in the Total Environment Simulator (TES) at the University of Hull in a $11\,\mathrm{m} \times 1.6\,\mathrm{m}$ flume with a flow depth 0.6 m. The rotor centre positioned at a depth of 0.307m to have a sufficient distance from the free surface. The experiment was carried out for a water speed U = 0.33m/s and a rotational rate $\Omega = 162.3\,\mathrm{rpm}$ resulting in a local chord-based Re about 30,000 at 0.75 blade span.

Unsteady simulations were carried out in a domain of size 5.5 m × 1.0 m × 0.6 m. A Cartesian structured mesh of 2.8×10^6 grid points with a resolution nearly R/30 in the turbine plane is used for the simulations. R is the rotor radius. Figure 1 shows a vertical slice of the mesh at the rotor axis plane. Numerical experiments [26, 27] showed that a cell size equal to R/30 is sufficient to have grid-independent results for the LES/ALM simulations. The rotor centre location is at a section 1.5 m from the inlet with a height 0.307 m from the bed. The time step is chosen to be 10^{-3}R/U corresponding to the azimuth step 0.3° and simulation is carried out for a total of 80.41 s. The statistics are averaged for the last 50 s to eliminate the effect of initial transience and get statistically stationary mean results. The simulation was run for 6200 core-hours. To avoid using a very fine mesh and increasing computational cost, the larger scales are not resolved near the bed and the short cylinder modelling the nacelle; instead, a wall model developed based on the Spalding's law [29] is used. In this simulation, the calculated y^+ for cells near the bed and the cylinder are approximately 4 and 12 respectively.

Applying the mapping technique [30, 31], turbulent inflow conditions are numerically generated at the inlet boundary and the zero normal gradient is applied for the velocity at the outlet. At the upstream boundary the normal pressure gradient is set to be zero and a constant pressure is applied on downstream. The side walls are treated as periodic boundaries. The channel bed and the cylinder are modelled as no slip walls and a free-slip condition is applied to the top boundary [32].

The mapping technique developed by Ahmadi & Tabor [30, 31] for LES is applied to generate the inflow conditions and for this simulation the mean and turbulent profiles experimentally measured for a turbulent flow in the plain flume (without the rotor and support) are used as the target profiles [23]. As shown in [23] the mapping technique can be cosidered as a fairly reliable method for generating inlet conditions for TST simulations with some shortcomings that still remain to be addressed.

Since there were no experimental data available for lift and drag coefficients (C_L and C_D) for the simulated rotor, these data were numerically generated for all blade sections at corresponding Reynolds numbers using XFOIL [33]. XFOIL has been validated against experimental data and other numerical techniques at low, moderate and high angles of attack [34, 35, 36]. Its reliability for using in this study has been validated with comparison against experimental data in [23].

3. RESULTS AND DISCUSSION

This study aims to examine the turbulence characteristics behind the turbine. Although the mean components provide a general view of the flow structure, turbulence characteristics give more details about the flow field especially the transition region behind the turbine. The numerical results of the present simulation have already been validated against the experimental data in [23]. Numerical Results are presented in a cylindrical coordinate system. Mean streamvise (v_x), tangential (v_θ) and radial (v_r) velocity components, rms velocity components, v'_x, v'_θ and v'_r are presented along the streamwise direction. The turbulent kinetic energy along the radial and streamwise directions are presented as well. The experimental data by Jordan

et al. [14] are referred to as the benchmark. In this paper, the bulk inlet velocity, U = 0.33 m/s and the rotor diameter, D = 0.2 m are used to normalise the quantities. The presented results are for the test case with a clockwise rotational speed $\Omega = 162.3$ rpm when looking downstream. Numerical results are compared with the experimental data measured at the vertical centre plane of the channel between $x = -0.16D$ and $x = 5D$ along the streamwise direction and between $z = -1.53D$ and $z = 1.5D$ in the vertical direction. The results are presented at two radii 0.98R and 0.82R to investigate the wake structure at two regions; a) around the blade tip vortices region at 0.98R and b) the inner region of the wake at 0.82R.

3.1. Mean flow

The normalised streamwise, tangential and radial mean velocity components in the streamwise direction at the vertical centre plane are presented in Figure 2 at the top, middle and bottom frames respectively. The plots depict the experimental and numerical results at two radii 0.98R and 0.82R below the rotor axis. As shown in the figure, the flow rate decreases as the fluid passes through the turbine and there is particularly a large flow rate deficit immediately behind the turbine. As the plots show the flow starts to recover further downstream but the wake is not fully recovered into its initial flow rate at the end of the domain.

Despite the reasonably good agreement for the predicted streamwise and radial mean velocity components near the turbine plane, the comparison shows a large deviation from experimental data for the tangential velocity component at this location. The experimental data for u_θ indicate that near the turbine plane water corotates with the rotor but further downstream it counter-rotates with the rotor as already reported for wind turbines in Refs. [37, 38, 10]. The flow rotates in the opposite direction to the rotor in reaction to the torque exerted by the flow on the rotor but a portion of the flow near the blade corotates with the blade due to the viscosity. Since in the ALM technique the blade and its boundary layer are not resolved, the numerical simulation can not predict the corotation region in the flow field. The discrepancies appeared in numerical results further downstream are mainly related to the simplifications used in the numerical simulation where the support is not modelled and nacelle is replaced with a short cylinder. As reported by Elie *et al.* [39] those discrepancies can be neglected further downstream from x/D = 5. For details about the vertical distributions of mean velocity components the reader is referred to [23].

3.2. Turbulent flow field

Figure 3 presents the rms velocity components and Turbulent Kinetic Energy defined as $\mathrm{TKE} = \frac{1}{2}(\mathrm{u'^2} + \mathrm{v'^2} + \mathrm{w'^2})$ in the streamwise direction downstream of the turbine at radii 0.98R and 0.82R below the rotor axis respectively. The numerical and experimental results show two peaks for velocity fluctuations and, in turn, TKE along the streamwise direction; the first peak at the turbine plane and the second one about 3D downstream. The comparison shows that the numerical simulation predicts the peak locations with a high degree of accuracy. The plots in Figure 3 show that while the numerical results for v'_x and v'_θ correlate well with the experimental data at the first peak for both radii 0.98R and 0.82R, the results for v'_r and, in turn, TKE at

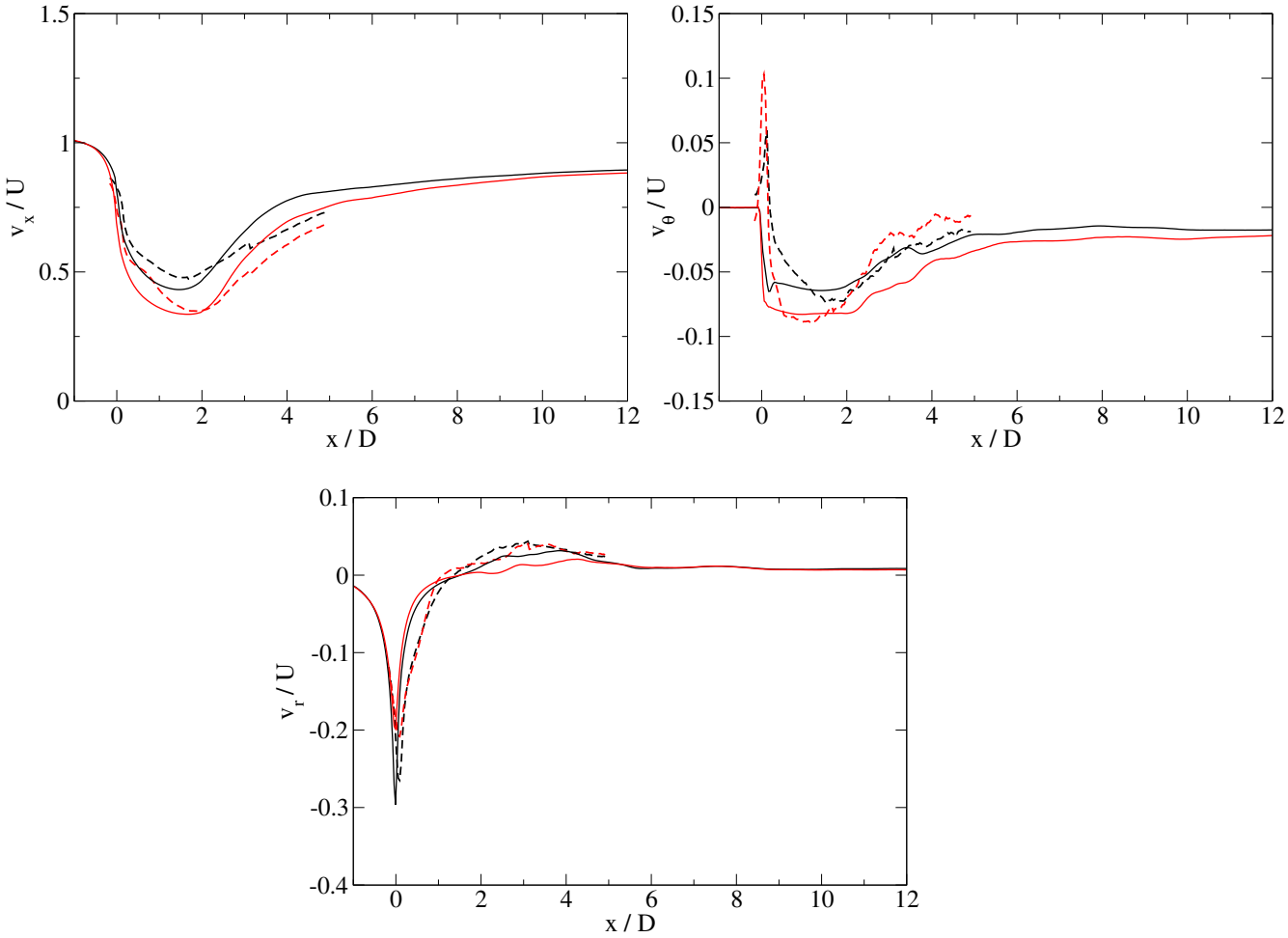

Figure 2: Streamwise (v_x), tangential(v_θ) and radial (v_r) mean velocity components at radii 0.98R (Black lines) and 0.82R (Red lines) below the rotor axis; Experiment: dashed-lines and CFD: solid-lines.

radius 0.82R show large deviations from the experimental data. The results shown at the first peak will be examined in detail later in Section 3.3.

At the second peak, the numerical results show good agreements with the experimental data except for v'_θ which are around 9% overestimated. The plots in Figure 3 show that in a region starting immediately behind the turbine, the measured turbulence level is higher than the predictions. The discrepancies can be related to the mechanical turbulence (the turbulence generated by the blades' boundary layer and vibrations) fed to the flow in the real case which is absent in the numerical simulation because of using the ALM technique in this study [40]. The plots also show that there is a transition to a highly turbulent flow in a region from 1.5D to 3D downstream. Of course, as plots show, because of a higher turbulence level, the transition starts sooner in the experiment. The flow characteristics of this region will be examined in detail later in the following section.

The plots presented in Figure 3 provide a better view of the evolution of the turbulence in the flow field behind the turbine. These plots can be used to explain the discrepancies appeared at locations 1D and 2D in

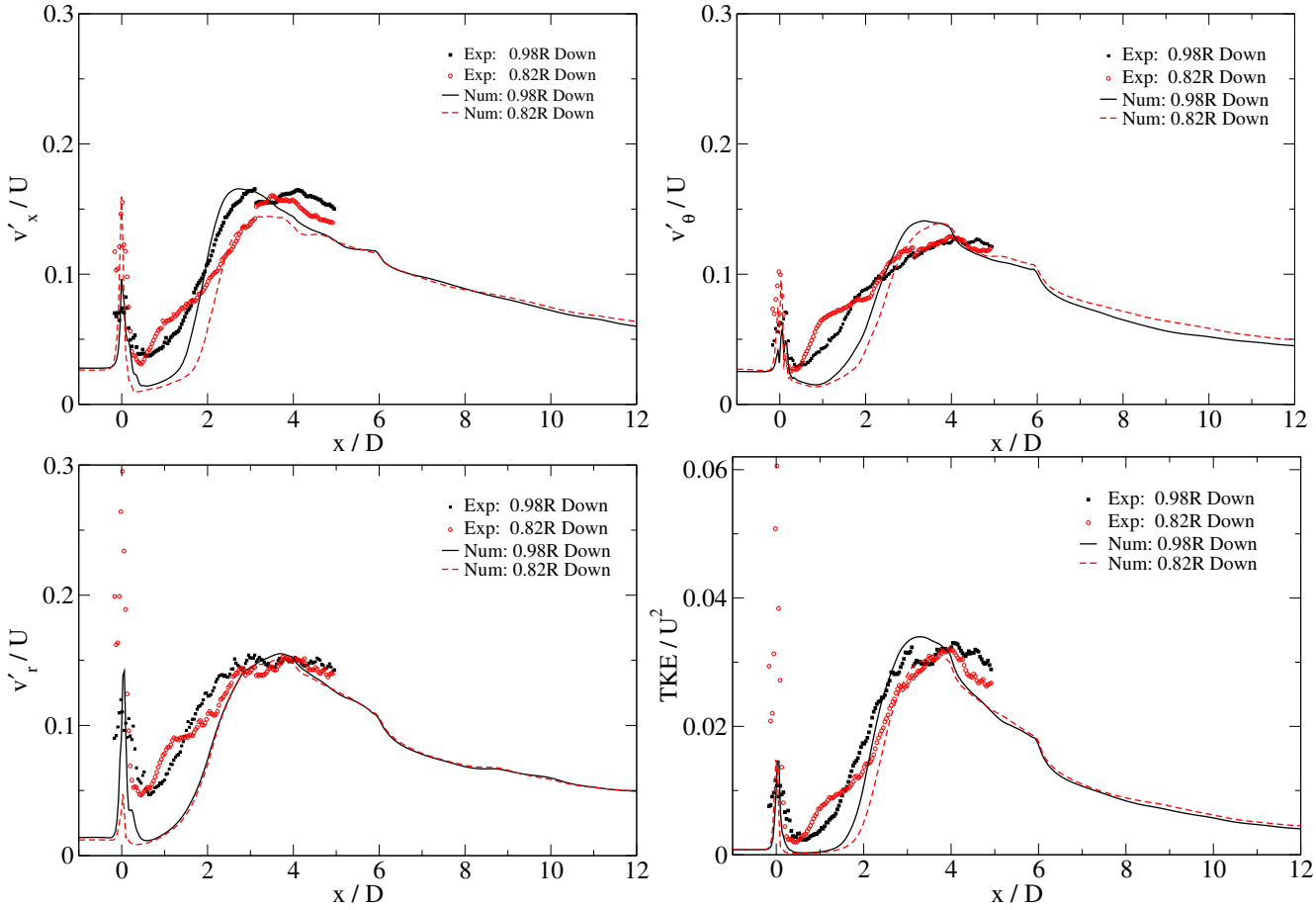

Figure 3: Streamwise (v'_x), tangential (v'_θ) and radial (v'_r) rms velocity components and turbulent kinetic energy in the streamwise direction behind the turbine at radii 0.92R and 0.82R below the rotor axis.

Figure 4. This figure already presented in [23] presents the vertical distributions of TKE at the vertical centre plane at locations 1D, 2D, 3D, 4D and 5D downstream of the turbine for the same simulation. As can be seen in Figure 4 while the plots show a very good agreement between CFD and experimental results at locations 3D and 4D, there are some deviations from the experimental data at heights higher than $z/D = -0.5$ at locations 1D and 2D behind the turbine. The discrepancies at locations 1D and 2D could be due to the mechanical turbulence as already described above. The excellent agreement seen at places 3D and 4D in Figure 4 is mainly due to their locations as shown in Figure 3 which are a highly turbulent region, where the mechanical turbulence generated by the turbine blades loses its importance. For analysing the rms velocity components and Reynolds shear stresses in the vertical direction, the reader is referred to [23].

Figure 5 presents iso-surfaces of the second invariant of the velocity-gradient tensor (Q), showing instantaneous vortex structures in the flow field coloured by the mean velocity. It can be seen from this figure that the stream of tip vortices from each blade merge into a cylindrical sheet of rotating turbulence and much of the periodic nature of the flow is lost as they mix and diffuse through the flow demonstrating clearly a flow regime transition. Considering the plots presented in Figure 3 together with the flow field depicted in

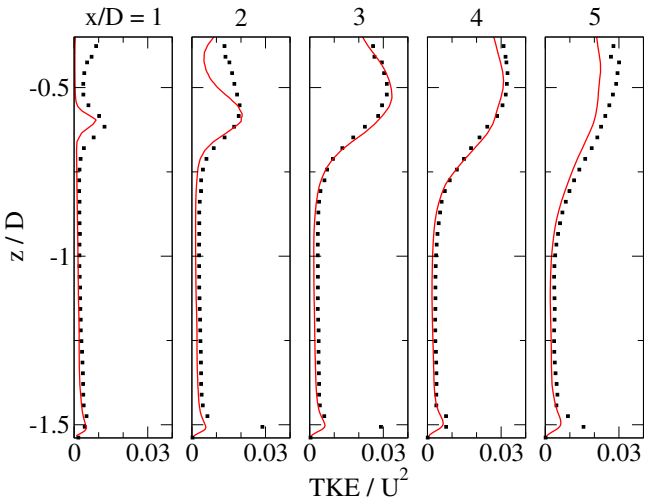

Figure 4: Turbulent kinetic energy downstream at the vertical centre plane; squares: Exp., solid lines: CFD [23].

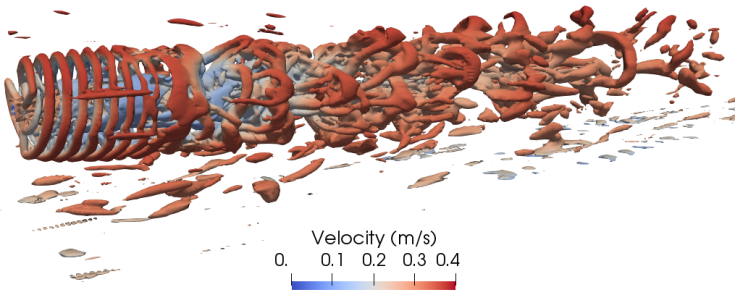

Figure 5: Instantaneous view of the mean velocity and vortex structures in the flow field.

Figure 5, it shows that the second peak of the plots is generated by the breakdown of tip vortices. In fact, the axial location of the second peak represents the streamwise location of the tip vortex breakdown in the domain which will be explained in more detail later in Section 3.3. Since the wake recovery starts by the hub/tip vortex breakdown in the domain, flow characteristics at this section will strongly affect the wake recovery, its rate and the turbulence intensity further downstream. In other words, since the flow regime between two peaks generates the initial conditions for downstream flow, a better understanding of this region is necessary. Despite its importance, this region is often absent or partly covered in most experimental studies [3, 4, 7] due to practical restrictions and numerical simulations using ADM and BEM techniques [15] because of their nature and weakness in predicting hub/tip vortices. Therefore, in most published works the presented data and relevant analyses suffer from incomplete coverage of the flow filed upstream of the transition region. A closer look at this region is presented in the following section.

3.3. Filtering velocity fluctuations

Although both numerical and experimental results presented in Figure 3 show two peaks in the streamwise direction for velocity fluctuations, a closer look at the results reveals that the first peak is mainly related to the deterministic velocity fluctuations (DVFs) and not the turbulent fluctuations. In experiments and numerical simulations, the rms velocity at a point is usually determined by calculating the standard deviation of velocity fluctuations using the time-averaged mean velocity at that point. This approach is not valid to apply at the turbine plane and a narrow zone around it due to the periodic nature of flow resulted from the turbine rotation. In experimental studies, the phase-locked ensemble average proposed by Gostelow [18] is used to overcome this problem. Filtering out DVFs will provide a clearer view of the turbulent characteristics of flow passing the turbine.

Figure 6 presents numerical results for instantaneous velocity components at the turbine plane and a cross-section at 0.5D downstream at radii 0.98R and 0.82R. For each velocity profile shown in Figure 6, the

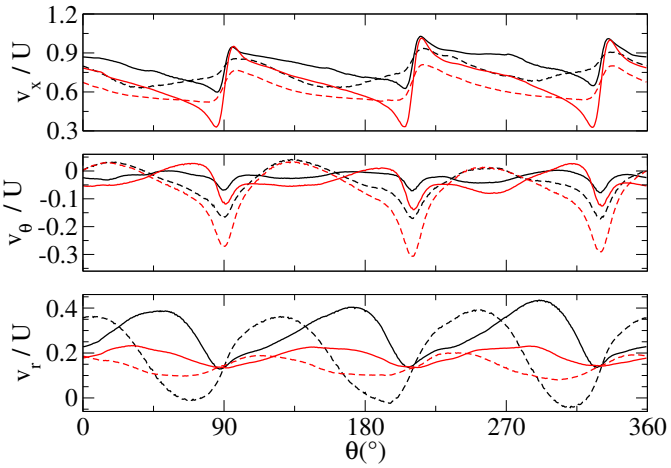

Figure 6: Instantaneous velocity components at radii 0.98R (Black lines) and 0.82R (Red lines) at the turbine plane (solid lines) and 0.5D downstream (dashed-lines).

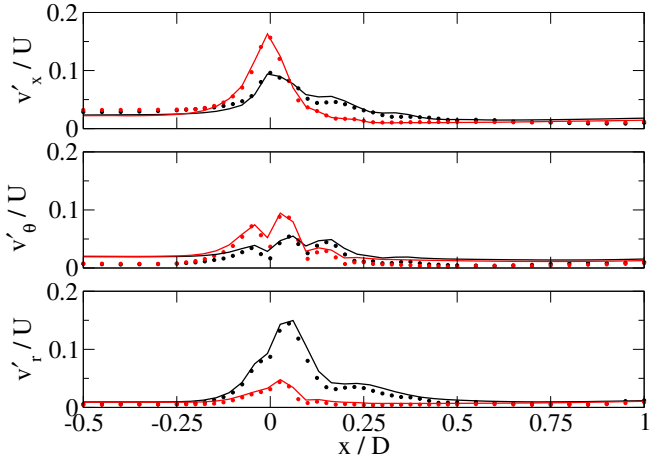

Figure 7: Space-averaged (circles) and time-averaged (solid-lines) velocity fluctuations at radii 0.98R (Black) and 0.82R (Red) in the streamwise direction.

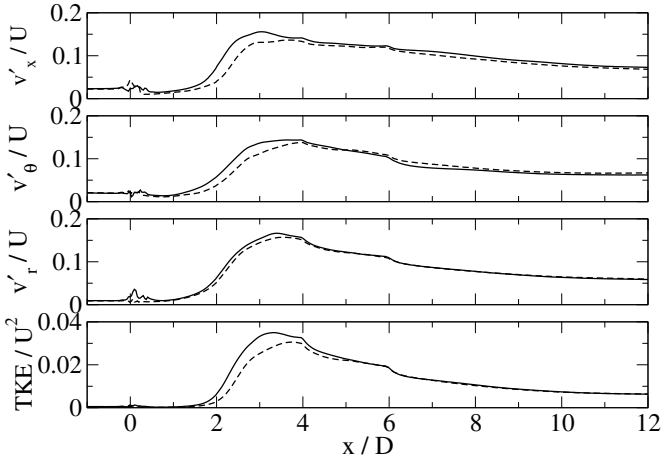

Figure 8: Filtered rms velocity components and TKE in the streamwise direction at 0.92R (solid-lines) and 0.82R (dashed-lines) below the rotational axis.

mean value and standard deviation can be calculated by space-averaging. The standard deviations calculated by space-averaging for three instantaneous velocity components at two radii 0.98R and 0.82R are presented in Figure 7 by symbols for 45 cross sections between 0.5D upstream up to 1D downstream of the turbine. In Figure 7 the rms velocity components calculated by time-averaging are also presented (solid lines) for radii 0.98R (black) and 0.82R (red) to make a comparison. It can be seen that there are very good agreements between rms velocity components calculated by the space- and time-averaging, confirming that the first peaks seen in Figure 3 are actually caused by deterministic and not turbulent velocity fluctuations. It is evident from the above discussion that the rms velocity components and TKE presented in Figure 3 contain both deterministic and turbulent velocity fluctuations and to get a clear view of turbulent fluctuations, DVFs should be filtered out.

The velocity fluctuations are filtered by subtracting the space-averaged velocity fluctuations from the

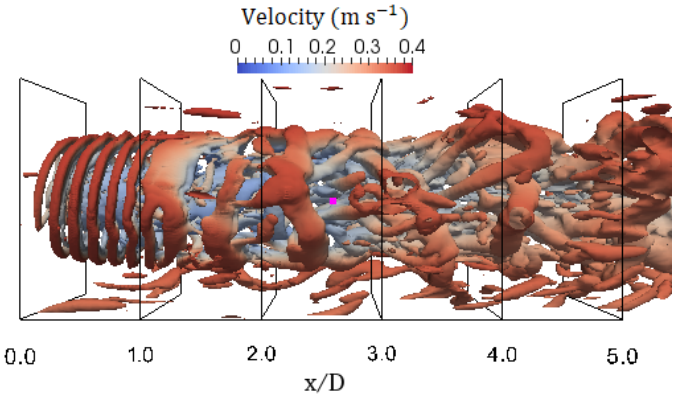

Figure 9: Instantaneous view of the flow field (a close-up).

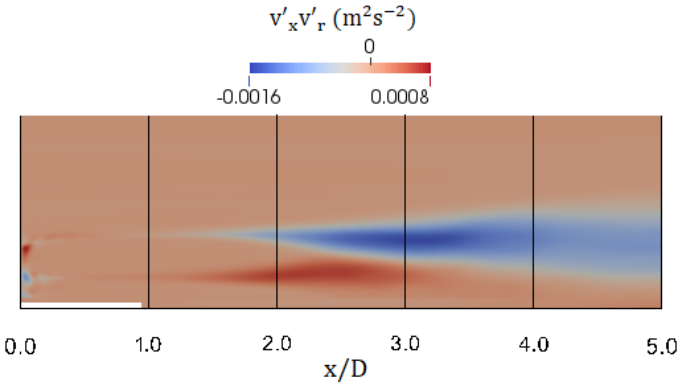

Figure 10: Shear stresses $v'_x v'_r$ at the top half of the vertical centre plane downstream.

time-averaged velocity fluctuations. The filtering process removes DVFs and gives turbulent fluctuations. Figure 8 presents the rms velocity components and TKE after filtering. The filtered profiles provide a better view of the turbulence characteristics of the flow passing the turbine. They show that the turbulent intensity is more or less constant through the turbine plane implying that the turbine does not affect the the turbulence level of the flow passing it when changing its direction from parallel to swirling. Of course, in a real case, because of the mechanical sources of turbulence which are absent in the ALM technique, the flow experiences a small increase in its turbulence level. But it would be ignorable in comparison to the removed DVFs as can be seen in Figure 3.

The distinction between these two peaks has to be considered when discussing about the turbulence characteristics downstream, particularly the decay rate of turbulence intensity. As Figures 5 and 8 show the main source of turbulence further downstream is coming from the process of tip (and hub) vortices breakdown and not the turbine. From Figure 8, three zones can be recognised in the flow field. The first zone is the region between the turbine plane and a section at about 1.5 D downstream with a nearly constant turbulence intensity. The second zone is approximately bounded between two planes at 1D and 3D downstream where the flow experiences an increase in its turbulence level. The third zone starts from the peak section with a monotonously decreasing behaviour in the turbulence intensity. The second zone itself can be divided in two sub-zones considering how the turbulence level varies; a region bounded between 1D and 1.8D with a gradual slope and a region bounded between 1.8D and 3D with a steep slope.

Figure 9 shows the flow structures at different zones explained above. This figure presents a close-up view of the flow field already shown in Figure 5. Comparing Figures 8 and 9 shows that the first zone represents the flow region consisting of the vortex tubes emitted from the blade tips. The second zone represents the region of the flow covering vortex sheets. The first sub-zone nearly starts at where the vortex tubes merge to a cylindrical sheet and covers the stable vortex sheets. The vortex sheets in the second sub-zone suffer from some instabilities resulting in vortex breakdown near the end of the zone. Figure 9 shows that the third zone represents the flow field behind the tip vortices breakdown. As mentioned before, in most experimental

studies and numerical simulations using ADM and BEM, the first and second zones are absent or partly covered while the variation rate of turbulence intensity particularly in the second zone strongly influences the peak location and its value, the wake recovery and the turbulence level in the third zone. A better understanding of flow field in the first and second zones is necessary to elucidate changes appeared in the flow characteristics downstream of the turbine caused by different upstream and operation conditions.

Different regions classified above are also visible in Figure 10. This figure depicts the shear stress $\mathrm{v'_x v'_r}$ at the top half of the channel vertical centre plane. This quantity is mainly related to the vertical transport of momentum in flow field. The negative values of shear indicate a momentum transport from the surrounding flow to the inner region of the wake resulting in re-energising it [41]. In the region near the turbine, the shear stress is concentrated in a thin layer at the wake border which corresponds to the first region discussed above with a nearly constant turbulence intensity. At the border of the wake, the shear stress has a negative value (white colour). The shear stress layer becomes thicker when instabilities occur in the wake. This region corresponds to the second zone shown in Figure 8 where the turbulence level of the flow increases quickly. Two sub-zones shown in Figure 8 are also recognisable here. As appeared in the figure, in the flow region between 1D and nearly 1.8D the shear layer becomes thicker slowly but after that up to 3D downstream it experiences a fast increase in thickness. The dark blue region in the figure represents the streamwise location of the turbulence intensity peak shown in Figure 8. Considering the common definitions of the near and far wake, the third zone introduced in this study represents the far wake with the turbulence peak location as its upstream boundary.

The plots presented in Figure 7 could be helpful to examine the unexpected large discrepancies seen in Figure 3 for predicted v'_r and in turn TKE. Considering the results presented in Figure 7 for three components v'_x, v'_θ and v'_r, and the results shown in Figure 3 for v'_x and v'_θ suggests that the discrepancies seen for v'_r should not be related to turbulent fluctuations. Because it is unusual to have turbulent fluctuations with only one non-zero component. Therefore the above deviations would be related to DVFs. There are three possible sources for these differences; ignoring the support in numerical simulation, inaccuracy or error in measurements and an unknown phenomenon in the flow. More information are needed for explaining this situation clearly.

4. Conclusion

A laboratory-scale three-bladed horizontal axis turbine was numerically simulated using the hybrid LES/ALM technique to investigate the evolution of turbulence characteristics downstream of the turbine. Deterministic velocity fluctuations stemmed from the turbine rotation were removed to achieve a better tracking of turbulent fluctuations and kinetic energy in the domain and have a clearer view of changes in the flow structure downstream. After filtering out DVFs, plots reveal a transition zone started shortly behind the turbine, resulting in a flow regime transition with a peak in the turbulence intensity. The variation rate of turbulence intensity in the transition zone strongly influence the turbulence peak location and value and,

in turn, the wake recovery and the turbulence level further downstream. Therefore, a better understanding of flow field in the transition zone is necessary to clarify changes in the wake characteristics caused by different upstream and operation conditions. This study also shows that the turbine wake can be split into distinct regions according to the streamwise variations of the turbulence intensity.

Comparing the numerical results to experimental data also demonstrates that the LES/ALM method can be used as an accurate and practical numerical technique for TST simulations, making it as a potentially good choice to apply for simulating tidal arrays.

Acknowledgements

Authors would like to thank Prof Ping Dong at the University of Liverpool for his great support, Prof. Daniel R. Parsons and his group at the University of Hull for providing the experimental data and Prof. Richard Brown and his group at the University of Strathclyde for the blade geometry. This work was funded by the Supergen Marine Challenge Programme of the EPSRC (EP/J010359/1).

References

[1] I. Afgan, J. McNaughton, S. Rolfo, D.D. Apsley, P. Stansby, Turbulent flow and loading on a tidal stream turbine by LES and RANS, International Journal of Heat and Fluid Flow 43 (2013) 96–108.

[2] S. Kang, X. Yang, F. Sotiropoulos, On the onset of wake meandering for an axial flow turbine in a turbulent open channel flow, J. Fluid Mech. 744 (2014) 376–403.

[3] S. C. Tedds, I. Owen, R. J. Poole, Near-wake Characteristics of a Model Horizontal Axis Tidal Stream Turbine, Renewable Energy 63 (2014) 222–235.

[4] L. Chamorro, D. R. Troolin, S. Lee, R. Arndt, F. Sotiropoulos, Three-dimensional flow visualization in the wake of a miniature axial-flow hydrokinetic turbine, Exp. Fluids 54:1459.

[5] M. Nuernberg, L. Tao, Experimental study of wake characteristics in tidal turbine arrays, Renewable Energy 127 (2018) 168–181.

[6] A. S. Bahaj, L. E. Myers, The effect of boundary proximity upon the wake structure of horizontal axis marine current turbines, Offshore Mechanics and Arctic Engineering 134 (2012) 021104:1–8.

[7] Y. Chen, B. Lin, J. Lin, S. Wang, Experimental study of wake structure behind a horizontal axis tidal stream turbine, Applied Energy 196 (2017) 82–96.

[8] T. Stallard, R. Collings, T. Feng, J.Whelan, Interactions between tidal turbine wakes: experimental study of a group of three-bladed rotors, Phil Trans R Soc A 371.

[9] D. Medici, P. Alfredsson, Measurements on a wind turbine wake: 3D effects and bluff body vortex shedding, Wind Energy 9 (2006) 219–236.

[10] M. Sherry, J. Sheridan, D. L. Jacono, Characterisation of a horizontal axis wind turbines tip and root vortices, Exp Fluids 54(3) (2013) 1–19.

[11] A. Ozbay, W.Tian, H. Hu, An experimental investigation on the aeromechanics and near wake characteristics of dual-rotor wind turbines (DRWTs), J. of Engineering for Gas Turbines and Power 138(4) 2014.

[12] M. Abkar, F. Porte-Agel, Influence of atmospheric stability on wind-turbine wakes: A large-eddy simulation study, Physics of Fluids 27 (3).

[13] S. Xie, C. L. Archer, A Numerical Study of Wind-Turbine Wakes for Three Atmospheric Stability Conditions, Boundary-Layer Meteorology 165 (2017) 85–112.

[14] L. Jordan, S. Simmons, S. McLelland, D. Parsons, L. Vybulkova, *The impact of tidal stream turbines on 3D flow and bed shear stress measured with particle image velocimetry in a laboratory flume*, In Proceedings of The 11th European Wave and Tidal Energy Conference (EWTEC) Nantes, France, Sept. 2015.

[15] W. M. J. Batten, M. Harrison, A. S. Bahaj, Accuracy of the actuator disc-RANS approach for predicting the performance and wake of tidal turbines, Phil Trans R Soc A 371 (2016) 1–15.

[16] K. Nilsson, W. Z. Shen, J. N. Sørensen, S. P. Breton, S. Ivanell, Validation of the actuator line method using near wake measurements of the MEXICO rotor, Wind Energy 37 (3) (2015) 499–514.

[17] L. A. Martinez, S. Leonardiy, M. J. Churchfield, P. J. Moriarty, A comparison of actuator disk and actuator line wind turbine models and best practices for their use, 50th AIAA Aerospace Sciences Meeting including the New Horizons Forum and Aerospace Exposition 09 - 12 January 2012, Nashville, Tennessee.

[18] J. P. Gostelow, A new approach to the experimental study of turbomachinery flow phenomena, J. Eng. Power 99 (1) (1977) 97–105.

[19] J. M. F. Oro, R. Ballesteros-Tajadura, E. B. Marigorta, K. M. A. Díaz, C. S. Morros, Turbulence and secondary flows in an axial flow fan with variable pitch blades, J. Fluids Engineering 130 (2008) 041101–11.

[20] J. F. Manwell, J. G. McGowan, A. L. Rogers, *Wind Energy Explained*, John Wiley & Sons Ltd, 2nd Edition.

[21] L. E. Myers, A. S. Bahaj, Experimental analysis of the flow field around horizontal axis tidal turbines by use of scale mesh disk rotor simulators, Ocean Engineering 37 (2010) 218–227.

[22] M. H. B. Ahmadi, P. Dong, Validation of the actuator line method for simulating flow through a horizontal axis tidal stream turbine by comparison with measurements, Renew. Energy 113 (2017) 420–427.

[23] M. H. B. Ahmadi, P. Dong, Numerical simulations of wake characteristics of a horizontal axis tidal stream turbine using actuator line model, Renew. Energy 113 (2017) 669–678.

[24] S. Menon, P. K. Yeung, W. W. Kim, Effect of Subgrid Models on the Computed Interscale Energy Transfer in Isotropic Turbulence, Computers & Fluids 25 (2) (1996) 165–180.

[25] OpenFOAM, Released via the OpenFOAM Foundation, See http://openfoam.org.

[26] J. N. Sørensen, W. Z. Shen, Numerical Modelling of Wind Turbine Wakes, Journal of Fluids Engineering 124 (2002) 393–399.

[27] W. Z. Shen, W. J. Zhu, J. N. Sørensen, Actuator Line/Navier-Stokes Computations for The MEXICO Rotor: Comparison With Detailed Measurements, Wind Energy 15(5) (2012) 811–825.

[28] N. Troldborg, Actuator Line Modelling of Wind Turbine Wakes, PhD Thesis, Technical University of Denmark, Denmark (2008).

[29] A. Chaudhari, Large eddy simulation of wind flows over complex terrains for wind energy applications, Ph.D. Thesis, Lappeenranta University of Technology, Lappeenranta, Finland 2014.

[30] M. H. B. Ahmadi, G. R. Tabor, Inlet Conditions for Large Eddy Simulation of Gas-Turbine Swirl Injector, AIAA J. 46 (7) (2008) 1782–1790.

[31] M. H. B. Ahmadi, G. R. Tabor, Inlet Conditions for LES using Mapping and Feedback Control, Computers & Fluids 38 (2009) 1299–1311.

[32] C. A. Consul, R. H. J. Willden and S. C. McIntosh, Blockage effects on the hydrodynamic performance of a marine cross-flow turbine, Philosophical Transactions of the Royal Society A 371: 20120299.

[33] XFOIL, See https://stuff.mit.edu/afs/athena/software/aeroutil-v1.0/Xfoil.

[34] P. Fuglsang, I. Antoniou, N. Sørensen, H. A. Madsen, Validation of a wind tunnel testing facility for blade surface pressure measurements, Risø National Laboratory, Risø-R-981(EN), Denmark, 1998.

[35] P. Fuglsang, I. Antoniou, I. Bak, H. A. Madsen, Wind tunnel test of the Risø-1 airfoil, Risø National Laboratory, Risø-R-981(EN), Denmark, 1998.

[36] J. H. Zhang, Numerical modeling of vertical axis wind turbine (VAWT), Technical University of Denmark, MEK-FM-EP 2004-11, Denmark, 2004.

[37] F. Porte-Agel, Y. Wu, H. Lu, R. Conzemius, Large-eddy simulation of atmospheric boundary layer flow through wind turbines and wind farms, J. Wind Eng. Ind. Aerodyn 99 (2011) 154–168.

[38] H. Hu, Z. Yang, P. Sarkar, Dynamic wind loads and wake characteristics of a wind turbine model in an atmospheric boundary layer wind, Experiments in Fluids 52 (5) (2012) 1277–1294.

[39] B. Elie, G. Oger, P.-E. Guillerm, B. Alessandrini, Simulation of horizontal axis tidal turbine wakes using a Weakly-Compressible Cartesian Hydrodynamic solver with local mesh refinement, Renew. Energy 108 (2017) 336–354.

[40] S. R. Turnock, A. B. Phillips, J. Banks, R. Nicholls-Lee, Modelling tidal current turbine wakes using a coupled RANS-BEMT approach as a tool for analysing power capture of arrays of turbines, Ocean Engineering 38 (2011) 1300–1307.

[41] N. Hamilton, H. S. Kang, C. Meneveau, R. B. Cal, Statistical analysis of kinetic energy entrainment in a model wind turbine array boundary layer, J. Renew. Sustain Energy 4 (2012) 063105–19.